Journal of Magnetic Resonance **139,** 240–249 (1999)
Article ID jmre.1999.1764, available online at http://www.idealibrary.com on IDEAL®

In Vivo Detection of ^{15}N-Coupled Protons in Rat Brain by ISIS Localization and Multiple-Quantum Editing

Keiko Kanamori[1] and Brian D. Ross

Magnetic Resonance Spectroscopy Laboratory, Huntington Medical Research Institutes, 660 South Fair Oaks Avenue, Pasadena, California 91105

Received August 19, 1998; revised March 17, 1999

Three-dimensional image-selected *in vivo* spectroscopy (ISIS) was combined with phase-cycled ^{1}H–^{15}N heteronuclear multiple-quantum coherence (HMQC) transfer NMR for localized selective observation of protons *J*-coupled to ^{15}N in phantoms and *in vivo.* The ISIS–HMQC sequence, supplemented by jump–return water suppression, permitted localized selective observation of 2–5 μmol of [$^{15}N_{indole}$]tryptophan, a precursor of the neurotransmitter serotonin, through the ^{15}N-coupled proton in 20–40 min of acquisition *in vitro* at 4.7 T. *In vivo,* the amide proton of [5-^{15}N]glutamine was selectively observed in the brain of spontaneously breathing $^{15}NH_4^+$-infused rats, using a volume probe with homogeneous ^{1}H and ^{15}N fields. Signal recovery after three-dimensional localization was 72–82% in phantoms and 59 ± 4% *in vivo.* The result demonstrates that localized selective observation of ^{15}N-coupled protons, with complete cancellation of all other protons except water, can be achieved in spontaneously breathing animals by the ISIS–HMQC sequence. This sequence performs both volume selection and heteronuclear editing through an addition/subtraction scheme and predicts the highest intrinsic sensitivity for detection of ^{15}N-coupled protons in the selected volume. The advantages and limitations of this method for *in vivo* application are compared to those of other localized editing techniques currently in use for non-exchanging protons. © 1999 Academic Press

Key Words: **ISIS; ^{15}N–^{1}H HMQC; *in vivo;* rat; brain.**

INTRODUCTION

Selective observation of protons coupled to ^{13}C or ^{15}N by spin-echo-difference (*1–3*), B_1-insensitive spectral editing pulse (*4*), and gradient-enhanced (*5–7*) or phase-cycled (*8, 9*) heteronuclear multiple-quantum coherence (HMQC) transfer NMR permits indirect detection of ^{13}C- or ^{15}N-labeled metabolites with high sensitivity. A ^{1}H-observed, ^{13}C-edited (POCE) spin-echo method, combined with localization by ISIS using a surface or volume coil, has permitted measurement of the rate of the tricarboxylic acid cycle (*2, 10–12*) and of glutamate turnover (*1, 3, 13, 14*) in the human and animal brain. ISIS localization, combined with gradient-enhanced ^{1}H–^{13}C double-quantum editing (*6, 7*) or with B_1-insensitive spectral editing (*4*), has been useful for study of ^{13}C-metabolites in animal brain. Selective *in vivo* observation of [5-^{15}N]glutamine amide protons by phase-cycled ^{1}H–^{15}N HMQC in rat brain (*9*) has permitted kinetic studies of the rate of glutamine synthesis (*15, 16*) and of pH changes in the glial compartment (*17*). The ^{1}H–^{15}N HMQC studies were performed with a head probe with homogeneous ^{1}H and ^{15}N fields, but spatial localization was not necessary because [5-^{15}N]glutamine was shown, in a preliminary experiment (*18*), to arise exclusively from the brain.

For ^{1}H–^{15}N HMQC study of other brain ^{15}N-enriched metabolites that may also occur in adjacent tissues and for examination of major regional variations within the intact brain, spatial localization is necessary. A pulse sequence for spatially localized selective observation of ^{1}H coupled to ^{15}N has not been reported to date. Recent installation of strong shielded gradients on our 4.7 T magnet opened the way to spatial localization by frequency-selective RF pulses in the presence of B_0 gradients. Three common localization techniques based on this method are ISIS (*19*), point-resolved spectroscopy (PRESS) (*20, 21*), and stimulated-echo acquisition mode (STEAM) (*22–24*). Among these, ISIS results in the least T_2-induced loss in signal intensity, and is hence suitable for localized observation of ^{15}N-bound protons which may undergo base-catalyzed exchange with water protons. The rate of exchange, k, is pH- and temperature-dependent. The ^{15}N-bound protons that are observable by ^{1}H–^{15}N HMQC at physiological pH (7.1–7.2) and temperature (37°C) *in vitro* have negligible or very low k under that condition. However, the effects on k and T_2 of the intracellular environment and pH fluctuations *in vivo* have been examined only for [5-^{15}N]glutamine amide protons in rat brain (*17*). The corresponding effect on the ^{15}N-coupled protons of other brain metabolites which are also potentially detectable by this technique *in vivo*, such as [$^{15}N_{indole}$]tryptophan and the neurotransmitter [$^{15}N_{indole}$] serotonin (*25*), is unknown. If k is nonnegligible and T_2 is reduced *in vivo*, magnetization of exchanging protons decays with TE as $\exp[-TE(1/T_2 + k)]$ in PRESS and STEAM, and with TM as $\exp[-TM(1/T_1 + k)]$ in STEAM (*26*). In ISIS, on the other hand, the only T_2-induced signal loss occurs during the short selective inversion pulses (*27*).

For nonexchanging C-bound protons, PRESS and STEAM have been combined with a homonuclear gradient-enhanced

[1] To whom correspondence should be addressed. E-mail: soccss@hmri.org, Fax: 626-397-3332.

1090-7807/99 $30.00
Copyright © 1999 by Academic Press
All rights of reproduction in any form reserved.

double-quantum filter or with a MEGA pulse (*28*) for selective observation of *J*-coupled protons of lactate (*7, 29*), GABA (*28, 30*), and glucose (*31*) *in vivo.* The single-shot method minimizes localization and editing errors arising from interscan subject motion and is valuable for selective observation of proton signals that are normally overlapped by large unwanted signals. However, the gradient-enhanced double-quantum filter has only half the intrinsic sensitivity of the phase-cycled multiple-quantum filter which can select both zero- and double-quantum coherences (*32, 33*). Because detection sensitivity is of primary importance in indirect observation of low-concentration ^{15}N-labeled metabolites in the small rat brain, we have selected a combination of ISIS and phase-cycled HMQC which predicts the highest intrinsic sensitivity.

Another issue to be addressed in the localized observation of ^{15}N-bound protons is a water suppression method that is suitable for slowly exchanging protons, to supplement suppression achieved by the ^{1}H–^{15}N HMQC sequence. On-resonance water presaturation should be avoided since it can cause attenuation of the ^{15}N-bound proton signals by saturation transfer (*26, 34*). The jump–return sequence (*35, 36*) has been successfully used in our previous *in vivo* and *in vitro* ^{1}H–^{15}N HMQC studies (*9, 25*), but the effectiveness of this sequence, when combined with ISIS localization, is unknown.

We report here localized selective observation of ^{1}H coupled to ^{15}N by ISIS combined with phase-cycled HMQC and jump–return water suppression. Phantom studies demonstrate the effectiveness of the method for 3D-localized observation of ^{15}N-coupled protons in biologically interesting metabolites. Because susceptibility to motion, resulting in imperfect cancellation of unwanted signals and coaddition of selected signals, is considered to be a potential drawback of both ISIS (*37*) and phase-cycled HMQC (*5, 38, 39*) for *in vivo* application, we have tested the ISIS–HMQC sequence for localized selective observation of brain [5-^{15}N]glutamine amide proton in anesthetized, spontaneously breathing rats during $^{15}NH_4Ac$ infusion. The result shows that the method permits localized selective observation of ^{15}N-coupled protons *in vivo* with cancellation of all other protons except water.

EXPERIMENTAL PROCEDURES

Phantoms

Two-compartment phantoms consisted of an outer cylindrical NMR tube, 18 mm in inner diameter and filled with a 3-ml solution to 18 mm height, and a coaxial inner tube, 9 mm in inner diameter and filled with a 1-ml solution to 16 mm height. The first phantom contained an aqueous solution of 200 μmol of [3-$^{15}N_2$]arginine in the inner chamber and [$^{15}N_2$]urea (200 μmol) in the outer chamber (ARG–UREA phantom). The second phantom contained [$^{15}N_{indole}$]tryptophan (42 μmol) in the inner and [^{15}N]acetylaspartate (38 μmol) in the outer chamber (TRP–NAA phantom). In addition, a one-compartment phantom (9-mm-i.d. NMR tube with a 2.2-ml solution volume) containing 495 μmol of [5-^{15}N]glutamine was used (GLN phantom). All phantoms were at pH 7.1 (intracellular pH of the brain), except for [3-$^{15}N_2$]arginine, which was at pH 3.6 to minimize the rate of exchange of the ^{15}N-bound protons with water proton (*40*). All ^{15}N-labeled chemicals were from Cambridge Isotopes except for [^{15}N]acetylaspartate, which was synthesized as described previously (*25*).

Animal Preparation

Male Wistar rats (220–240 g) were prepared for intravenous infusion through the femoral vein as described previously (*41*). $^{15}NH_4Ac$ (1 M solution at pH 7.4) was infused at a rate of 5.0 $\pm$ 0.1 mmol/h/kg wt for 1.8 $\pm$ 0.1 h on benchtop. The anesthetized, spontaneously breathing rat was then placed in the ^{1}H–^{15}N probe with the head in a specifically designed holder to ensure immobility of the cranium, and infusion continued for an additional 5–6 h in the magnet for localized observation of brain [5-^{15}N]glutamine. At the end of the *in vivo* experiment, the rat was sacrificed and the brain frozen immediately in liquid nitrogen for preparation of a perchloric acid extract. The concentration of [5-^{15}N]glutamine in the brain extract was measured by direct ^{15}N NMR as described previously (*42*).

NMR

Localized ^{1}H–^{15}N HMQC spectra were obtained on a Bruker-GE CSI-II spectrometer, equipped with a 4.7-T Oxford magnet and a Bruker Acustar shielded gradient with a bore diameter of 180 mm and a maximum gradient strength of 95 mT/m. The probe, manufactured by Robert L. Domenick (Magnetic Resonance Plus, Sacramento, CA) and modified extensively by James Tropp (GE Medical Systems, Fremont, CA), consisted of separate, orthogonal resonators for ^{1}H (observe) and ^{15}N (decouple) as described previously (*9*). The probe was placed in the magnet with the ^{1}H (B_1) field oriented along the x axis and the ^{15}N field (B_2) along the vertical (y) axis, where z is the B_0 axis. The three-dimensional coordinates of the phantom and of rat brain were determined by imaging in the xy and yz planes by a spin-echo imaging sequence. Operating conditions were a FOV of 90 mm, a TE of 30 ms, a TR of 1 s, and a slice thickness of 3 mm (phantom) or 7 mm (brain). Brain water was shimmed to a linewidth of 27–37 Hz on a 20 mm (x) $\times$ 16 mm (y) $\times$ 10 mm (z) voxel by the STEAM sequence. Operating conditions employed a TE of 60 ms, a TM of 30 ms, and a TR of 4 s.

The pulse sequence for localized, selective observation of ^{1}H coupled to ^{15}N is shown in Fig. 1. Localization was performed by the ISIS sequence of Ordidge *et al.* (*19*). The selective inversion pulses were three-lobe sinc pulses of 1.5 ms (*in vivo*) or 1.75–1.9 ms (phantoms). A 0.5-ms delay (D1 in Fig. 1) was placed after the last slice select gradient to allow magnetic field stabilization before the ^{1}H excitation pulse. Coaddition of signals from the volume of interest (VOI) and subtraction of

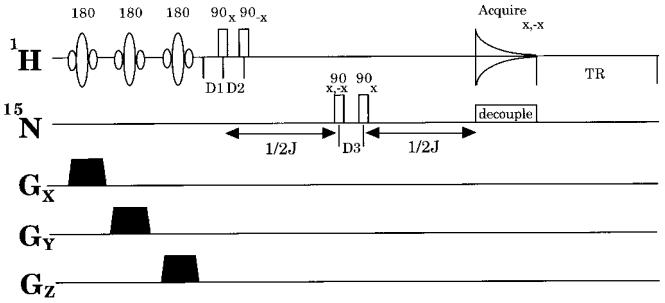

FIG. 1. The pulse sequence for ISIS–HMQC, supplemented by jump–return water suppression, for localized selective observation of ^{15}N-coupled protons by zero- and double-quantum filter. The frequency selective pulses for ISIS were three-lobe sinc pulses of 1.5 ms (*in vivo*) or 1.75–1.9 ms (phantoms). Water suppression was achieved by the ^{1}H $90°_{x}$–D2–^{1}H $90°_{-x}$ sequence. The ^{1}H and ^{15}N pulses in the HMQC sequence were hard pulses of 20–45 and 400–450 μs, respectively. The phase of each pulse is shown in subscript, and was constant if a single phase is shown. For the first ^{15}N pulse and the receiver, two phases are shown, reflecting the two-step phase cycling performed to select ^{15}N-coupled protons. D1 and D3 were 0.5 ms and 20 μs, respectively, and TR was 1 s. The values of D2 and 1/2J for each experiment are given in the text.

signals outside the VOI were performed by the eight-step addition/subtraction scheme of Ordidge *et al.* (*19*), with a minor modification in the order of experiments, so that the first four experiments perform 2D localization in the *xz* (instead of the *xy*) plane and the eight experiments perform 3D localization. Unlocalized spectra were obtained by omitting the selective inversion pulses.

Selective observation of ^{1}H coupled to ^{15}N was performed by the phase-cycled ^{1}H–^{15}N HMQC sequence, supplemented by jump–return water suppression, as described in detail previously (*9*), with the following two minor modifications. First, a two-step phase cycling of the first ^{15}N pulse and of the receiver was used, as shown by subscripts in Fig. 1. This is the minimum number required for selective observation of protons coupled to ^{15}N through zero- and double-quantum coherence selection and cancellation of other protons. All other pulses had constant phase. Second, the ^{1}H transmitter frequency was set on resonance for water, to achieve water suppression by the jump–return sequence while minimizing spatial displacement error for the ^{15}N-labeled compounds of interest. Water suppression is achieved when the second ^{1}H 90° pulse returns the water proton magnetization to the *z* axis. The magnetizations of ^{15}N-coupled protons of interest are not affected by this pulse because they undergo chemical shift evolution during D2 (0.69 ms for ARG, 0.23 ms for TRP, and 0.6 ms for GLN) and are aligned with the *x* axis when the second ^{1}H pulse is applied. Operating conditions employed a ^{1}H 90° pulse of 20–28.5 μs (phantoms) or 37–45 μs (*in vivo*), as optimized for each phantom or animal, a ^{15}N 90° pulse of 400–450 μs, a relaxation delay (TR) of 1000 ms, 1K data points, and a spectral width of 2000 Hz (GLN and ARG–UREA phantoms) or 2600 Hz (TRP–NAA phantom), with acquisition times of 256 or 196 ms, respectively. The preparation time (1/2J) was 5.56 ms for GLN (phantom and *in vivo*) and for the ARG–UREA phantom, and 5.25 ms for the TRP–NAA phantom, and D3 was 20 μs. ^{1}H chemical shifts are reported in parts per million from the methyl resonance of 2,2-dimethylsilapentane-5-sulfonic acid (DSS). The ^{15}N pulse was on resonance for [5-^{15}N]glutamine (−271 ppm from nitromethane, where the negative sign indicates upfield shift) for the GLN phantom and *in vivo*. For the two-compartment phantoms, the ^{15}N pulse was centered between the resonance frequencies of the respective phantom pairs (−306 ppm for [$^{15}N_2$]urea, −311 ppm for [3-$^{15}N_2$]arginine; −251 ppm for [^{15}N]acetylaspartate, and −253 ppm for [$^{15}N_{indole}$]tryptophan). ^{15}N decoupling was performed in the CW mode with a decoupler power (nominal output) of 40–50 W applied during the acquisition time.

For acquisition by ISIS–HMQC, *n* scans (typically 16 for phantoms and 176 *in vivo*) of HMQC acquisitions were performed per ISIS experiment and stored as FID. After one cycle of the eight ISIS experiments was completed, the process was repeated *N* times (typically 1–4) for signal averaging. This resulted in 8 × *N* stored FIDs, each consisting of *n* scans. These FIDs were sequentially added or subtracted according to

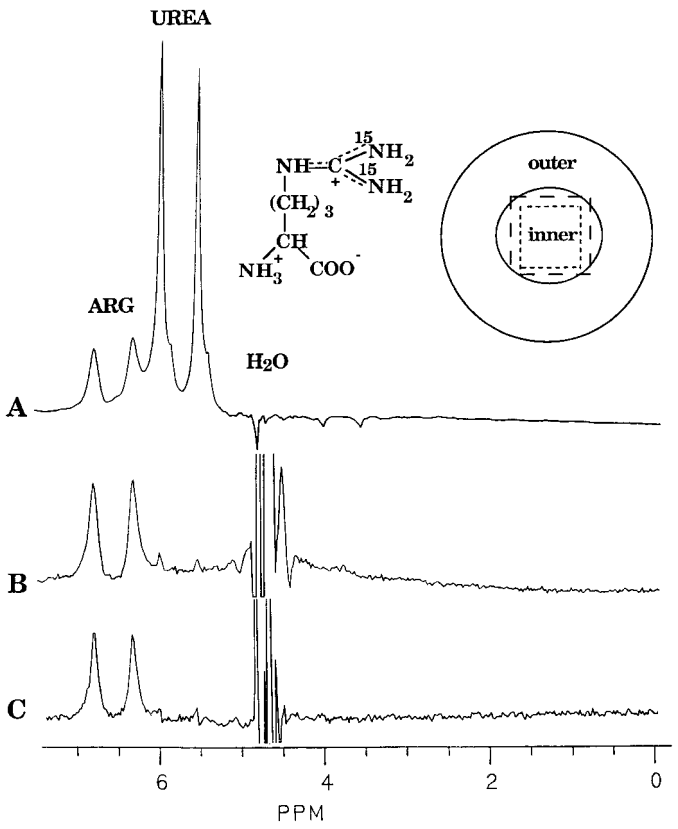

FIG. 2. ^{1}H–^{15}N HMQC spectra of a two-compartment phantom (*yz* plane shown in the inset) containing [$^{15}N_2$]urea in the outer and [3-$^{15}N_2$]arginine (structure in the inset) in the inner chamber, obtained (A) without localization, (B) from a 7 × 7 × 7-mm voxel (dashed line) and (C) a 5 × 5 × 5-mm voxel (dotted line) of the inner chamber.

TABLE 1
^{1}H Chemical Shifts, Coupling Constants, and Linewidths of ^{15}N-Bound Protons of Phantom Compounds at 200 MHz

	^{1}H chemical shift (ppm from DSS)			Linewidth (Hz)	
Compound	^{15}N-coupled	^{15}N-decoupled	$^{1}J_{^{15}N-^{1}H}$ (Hz)	^{15}N-coupled	^{15}N-decoupled
[3-$^{15}N_2$]Arginine	6.36		92	31	
	6.83				
[$^{15}N_2$]Urea	5.57		90	11	
	6.02				
[$^{15}N_{indole}$]Tryptophan	9.90	10.15	98	17	17–20
	10.40				
[^{15}N]Acetylaspartate, amide	7.78	8.01	92	18	30
	8.24		(7.9)[a]		
acetyl	1.97				
[5-^{15}N]Glutamine H_Z	6.67	6.9	90	9 ± 1	16–20
	7.11				
H_E	7.39	7.6	90	18 ± 4	27
	7.83				

[a] $^{3}J_{NH-H\alpha}$

the scheme of Ordidge *et al.* with the minor modification in the order of experiments described above. The resulting single FID contained signals from the ^{15}N-coupled protons in the selected VOI. Reported linewidths were measured without the application of an exponential filter.

Signal Recovery

Signal recovery in a localized spectrum was defined as $[A_{loc}/(A_{unloc} \times v/V)] \times 100\%$, where A_{loc} is the peak area of an ^{15}N-coupled proton observed from a voxel of volume v, and A_{unloc} is the peak area from the total volume V observed in the unlocalized spectrum. Hence the term $A_{unloc} \times v/V$ represents the peak area expected from the VOI if the selective inversion pulses for localization were 100% efficient.

RESULTS

In Vitro Studies

Figure 2A shows an unlocalized ^{15}N-coupled ^{1}H-^{15}N HMQC spectrum of the two-compartment phantom containing [3-$^{15}N_2$]arginine (see inset for structure) in the inner and [$^{15}N_2$]urea in the outer compartment. The chemical shifts of the ^{15}N-coupled resonances at 200 MHz and the coupling constants are listed in Table 1. The signals of arginine protons that are not coupled to ^{15}N (see, e.g., Roberts and Jardetzky (*43*) for chemical shifts) are suppressed, as is the water peak. The ^{15}N-bound arginine proton peaks are broad ($v_{1/2}$ of 31 Hz; Table 1) because the rotation of the ^{15}N–H groups around the C–N bonds, which have partial double-bond character, is not rapid enough at 20°C to completely average the chemical environments of the four ^{15}N-bound protons (*44*, *45*). Line broadening is not caused by chemical exchange of these protons with water protons because the rate of exchange is very slow at pH 3.6 (*40*). Figure 2B shows a localized spectrum obtained from a 7 × 7 × 7-mm voxel of the inner chamber (the voxel shown by the dashed line in the inset). While the [^{15}N]arginine protons are clearly observed, the urea peak area is reduced to 0.2% of that in Fig. 2A. In a spectrum obtained from a 16 × 7 × 7-mm voxel which closely approximates the dimension of the inner chamber along the *x* axis as well, the urea peak area was also very small, 1.4% of that in Fig. 2A (spectrum not shown). The spatial displacement error for [3-$^{15}N_2$]arginine protons, calculated from the chemical shift and the gradient strength, was 12%. In the spectrum obtained from a 5 × 5 × 5-mm voxel (Fig. 2C; voxel shown by the dotted line), the urea peak is barely detectable. The results show that the ISIS–HMQC sequence is effective for selective observation of ^{15}N-coupled protons from VOI.

To test the applicability of the method to brain metabolites at lower concentrations, spectra were obtained from a two-compartment phantom containing [$^{15}N_{indole}$]tryptophan (a precursor of the neurotransmitter serotonin) in the inner chamber and [^{15}N]acetylaspartate (a neuronal marker metabolite) in the outer chamber. In the unlocalized ^{15}N-coupled spectrum (Fig. 3A), the ^{15}N-bound proton of tryptophan is a doublet with $^{1}J_{^{15}N-^{1}H}$ of 98 Hz (Table 1). The amide proton of [^{15}N]-acetylaspartate is a doublet with $^{1}J_{^{15}N-^{1}H}$ of 92 Hz, and each doublet component shows a small splitting due to $^{3}J_{NH-H\alpha}$ of 7.9 Hz (*25*). The signal for the methyl protons of [^{15}N]-acetylaspartate at 1.97 ppm is also observed, indicating that the protons are coupled to ^{15}N, as is consistent with the reported $^{3}J_{CH_3-^{15}N}$ of 1.2 Hz for the structurally similar acetylalanine *N*-methylamide (*46*). With ^{15}N decoupling (Fig. 3B), the ^{15}N-bound indole proton of tryptophan is a singlet. The ^{15}N-decoupled amide proton of [^{15}N]acetyl-aspartate shows, as expected, the small three-bond coupling

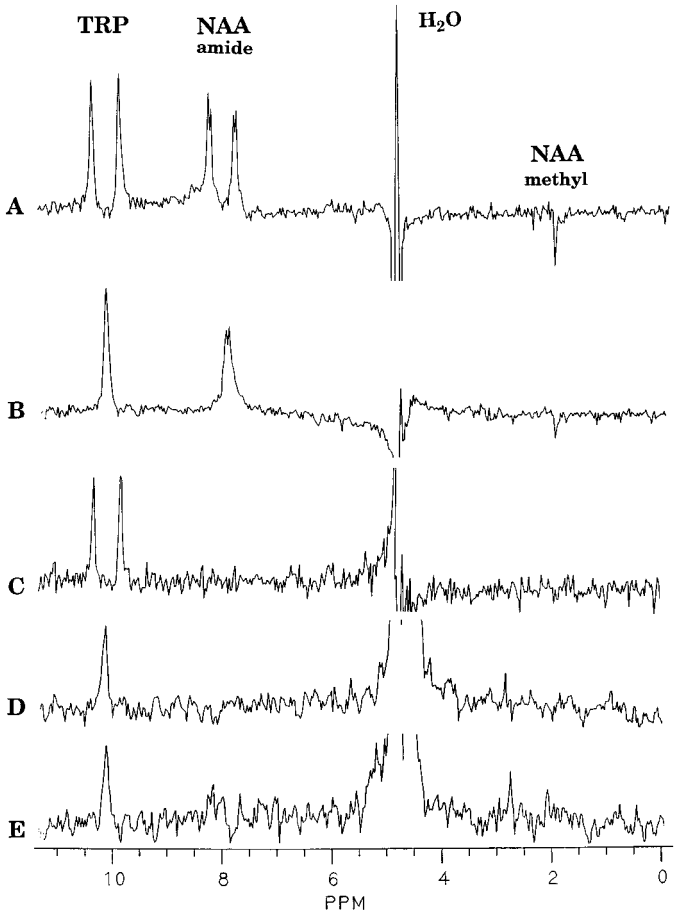

FIG. 3. $^{1}H–^{15}N$ HMQC spectra of a two-compartment phantom containing 42 μmol of [$^{15}N_{indole}$]tryptophan (TRP) in the inner and 38 μmol of [^{15}N]acetylaspartate (NAA) in the outer chamber. An unlocalized spectrum with ^{15}N coupling (A) shows selective observation of ^{15}N-coupled protons of both compounds; (B) the same obtained with ^{15}N decoupling. Localized spectra were obtained from a 5 × 5 × 5-mm voxel of the inner chamber containing 5.2 μmol of [^{15}N]TRP without (C) and with (D) ^{15}N decoupling in 26 min or (E) from a 4 × 4 × 4-mm voxel (2.6 μmol) in 41 min.

with the α-proton. Figure 3C shows a localized ^{15}N-coupled spectrum from the 5 × 5 × 5-mm voxel of the inner chamber. Only the ^{15}N-bound proton doublets of tryptophan are observed. Figure 3D shows a ^{15}N-decoupled spectrum obtained from the same VOI containing 5.2 μmol of [$^{15}N_{indole}$]tryptophan, acquired in 26 min. Figure 3E shows a corresponding spectrum from a 4 × 4 × 4-mm VOI containing 2.6 μmol acquired in 41 min. The results suggest that localized selective observation of ^{15}N-coupled protons at metabolite quantities of 2–5 μmol is feasible in 20–40 min of acquisition.

Figure 4A shows a ^{15}N-decoupled spectrum from a 5 × 5 × 5-mm voxel of the [5-^{15}N]glutamine phantom. The two amide protons, H_Z and H_E (see Figure inset), have chemical shifts of 6.9 and 7.6 ppm, respectively (*9*). The second amide proton H_E has a much lower signal intensity than H_Z *in vitro* at pH 7.1 and

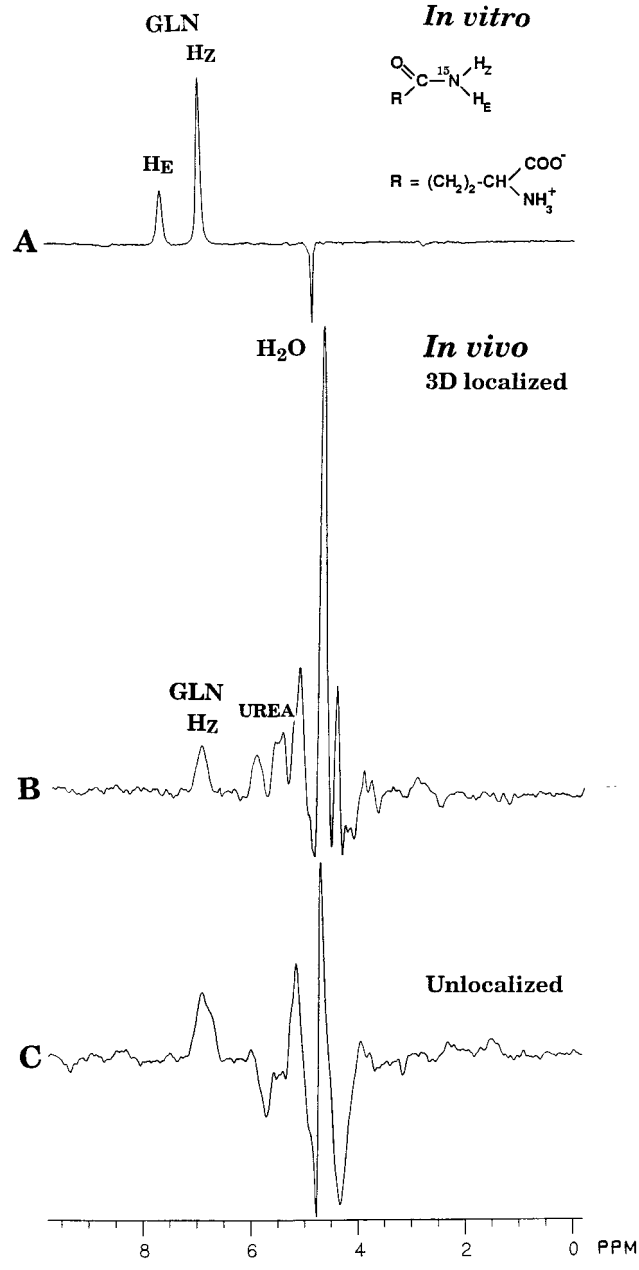

FIG. 4. $^{1}H–^{15}N$ HMQC spectra of [5-^{15}N]glutamine in a phantom and in rat brain *in vivo*. (A) A localized spectrum from a 5 × 5 × 5-mm voxel of a [5-^{15}N]glutamine phantom obtained with ^{15}N decoupling. The two amide protons H_Z and H_E (see inset for structure) are chemically nonequivalent. (B) An *in vivo* 3D-localized HMQC spectrum obtained from the brain of a spontaneously breathing $^{15}NH_4^+$-infused rat in 30 min. (C) An unlocalized *in vivo* spectrum acquired in 4 min. Exponential line broadening of 10 Hz was applied to (B) and (C). The slight offset between the water peak in the phantom (A) and the tallest residual water peak in the 3D-localized *in vivo* spectrum (B) arises from the fact that the ^{1}H carrier frequency was placed on shimmed phantom water (A) or brain water (B and C), and the residual water peak in (B) arose mainly from water in noncerebral tissues where B_0 was inhomogeneous. The chemical shift of [5-^{15}N]glutamine H_Z from the carrier frequency (and hence from brain water) in the *in vivo* spectra was 421 ± 4 Hz, which was virtually identical with that in the phantom, thus confirming the assignment of this peak.

20°C because (a) it exchanges at a faster rate with water protons than H_Z, resulting in a broader linewidth (Table 1), and (b) the acquisition condition, specifically the chemical shift evolution time, D2, is optimized for the observation of H_Z and not H_E.

In Vivo Study

Figure 4B shows a 3D-localized *in vivo* spectrum obtained from a 26 × 19 × 14-mm voxel of the brain of a spontaneously breathing $^{15}NH_4^+$-infused rat acquired in 30 min by the ISIS–HMQC sequence with ^{15}N decoupling. The corresponding unlocalized *in vivo* spectrum, acquired in 4 min, is shown in Fig. 4C. The voxel location is shown on the ^{1}H images of rat brain in Fig. 5 (*top*, transverse *xy* image; *bottom*, coronal *yz* image). The dimension of the brain was 23 mm (x) × 17 mm (y) × 11 mm (z) and the voxel circumscribes the brain and the surrounding skull, which has an average thickness of 1.5 mm on either side. The voxel was chosen to approximate the dimension of the brain for estimation of signal recovery (see Discussion). Noncerebral soft tissues were largely excluded except for the very small fraction which could not be eliminated due to the oval shape of the brain. In the *in vivo* spectra of Figs. 4B and C, the peaks in the 4.7 ± 0.6 ppm region represent residual water. Protons of brain metabolites that are not coupled to ^{15}N, such as the C-bound protons upfield of water, are suppressed by the phase-cycled HMQC sequence. In the region downfield of water, the prominent peak at 6.9 ppm can be assigned to the amide proton H_Z of brain [5-^{15}N]glutamine, by comparison with the *in vitro* spectrum in Fig. 4A. The linewidth of the H_Z peak was 38 ± 1 Hz (n = 2) in the 3D localized spectra and 40 ± 3 H_Z (n = 5) in the unlocalized spectra. At the physiological temperature of 37°C, the second amide peak H_E exchanges with water at a rate faster than that at 20°C, resulting in a broader linewidth (*17, 25*). Accordingly, H_E is not observed in the *in vivo* spectra of Figs. 4B and C. Brain [5-^{15}N]glutamine concentration in the *in vivo* spectrum (Fig. 4B), taken after 5.5 h of $^{15}NH_4$Ac infusion, was estimated to be approximately 9.2 μmol/g. This was determined from (a) the observed 30% increase in the peak area of the amide proton H_Z in the unlocalized *in vivo* spectra between t = 5.3 h and t = 7.3 h (just before sacrifice) and (b) brain [5-^{15}N]glutamine concentration of 11.9 μmol/g measured in the extract after sacrifice. Spatial displacement error, calculated from the chemical shift and the gradient strengths (6.4 mT/m along the z axis; 27% higher than in phantoms) was less than 8%.

The peaks at 5.6 and 6.0 ppm in the localized spectrum (Fig. 4B) arise from protons of [^{15}N]urea which is present in the brain of the $^{15}NH_4$-infused rat (*42*). The urea proton signals are not ^{15}N decoupled because the ^{15}N frequency of urea (35 ppm upfield of [5-^{15}N]glutamine) lies outside the CW decoupling bandwidth under the experimental conditions, which have been optimized for [5-^{15}N]glutamine observation, as has been demonstrated *in vitro* previously (*9*). It is to be noted that [$^{15}N_2$]urea has two equivalent protons per ^{15}N and four equivalent protons per molecule, compared to one amide proton H_Z per [5-^{15}N]glutamine molecule. Hence, the ratio of the proton peak areas of [$^{15}N_2$]urea to that of [5-^{15}N]glutamine in the *in vivo* ^{1}H spectrum is expected to be much higher than their actual concentration ratio in the brain. In the unlocalized ^{1}H spectrum (Fig. 4C) acquired in 4 min, the urea proton peaks are out of phase and broadened because B_0 was considerably less homogeneous in noncerebral tissues containing [$^{15}N_2$]urea; viz., the circulating blood and muscle within the probe ($v_{1/2}$ for whole-volume water was 140 Hz compared to 27–37 Hz for brain water). By contrast, in direct unlocalized *in vivo* ^{15}N NMR spectra of $^{15}NH_4$-infused rat, [^{15}N]urea in the tissues within the head probe was observed despite similar B_0 inhomogeneity over noncerebral tissues, because with γ_{15N}/γ_{1H} of 0.1, B_0 inhomogeneity causes much less line broadening (in Hertz) of ^{15}N than of ^{1}H signal. Brain [^{15}N]urea was not detected in the 3D-localized ^{15}N spectrum because [^{15}N]urea has one ^{15}N per two ^{1}H (*47*). The significance of the present *in vivo* result is that the amide proton of brain [5-^{15}N]glutamine, for which the acquisition conditions were optimized, was selectively observed with cancellation of all protons not coupled to ^{15}N.

Signal Recovery

To estimate signal loss in the localization process, signal recovery, as defined under Experimental Procedures, was measured for the [3-$^{15}N_2$]arginine and [5-^{15}N]glutamine phantoms and for brain [5-^{15}N]glutamine *in vivo*. For a two-compartment phantom, it has been suggested that signal recovery can most accurately be measured for a voxel that approximates the dimension of the (inner) chamber containing the test compound, because the slice-selective sinc inversion pulses are normally truncated, resulting in frequency profiles with side lobes that extend beyond the nominal bandwidth (*48*). In our study, the inner chamber was a cylinder of length 16 mm (x) and an i.d. of 9 mm (o.d. of 10 mm) in the yz plane. Hence, a rectangular voxel of 16 (x) × 7 (y) × 7 (z) mm was chosen. The edges of the voxel in the yz plane just touch the outer surface of the inner chamber, as shown by the dashed line in Fig. 2. This corresponds to a two-dimensional version of the optimum fit of a cubic voxel to a spherical sample, as described by Ernst *et al.* (*49*). The signal recovery for [3-$^{15}N_2$]arginine protons in this voxel was 72% (Table 2). The signal recovery was 82% for a 9 × 9 × 9 mm voxel; in the yz plane, this voxel circumscribes the inner chamber, which has an i.d. of 9 mm. The results suggest that signal recovery in a VOI which approximates the dimensions of the inner chamber is 72–82%. Hence, the efficiency of sinc inversion pulses along each of the three axes was about 90% *in vitro*. Signal recovery from smaller voxels was similar (Table 2). For [5-^{15}N]glutamine, signal recovery was also measured after increasing the relaxation delay from 1 s, a condition which optimizes the S/N ratio

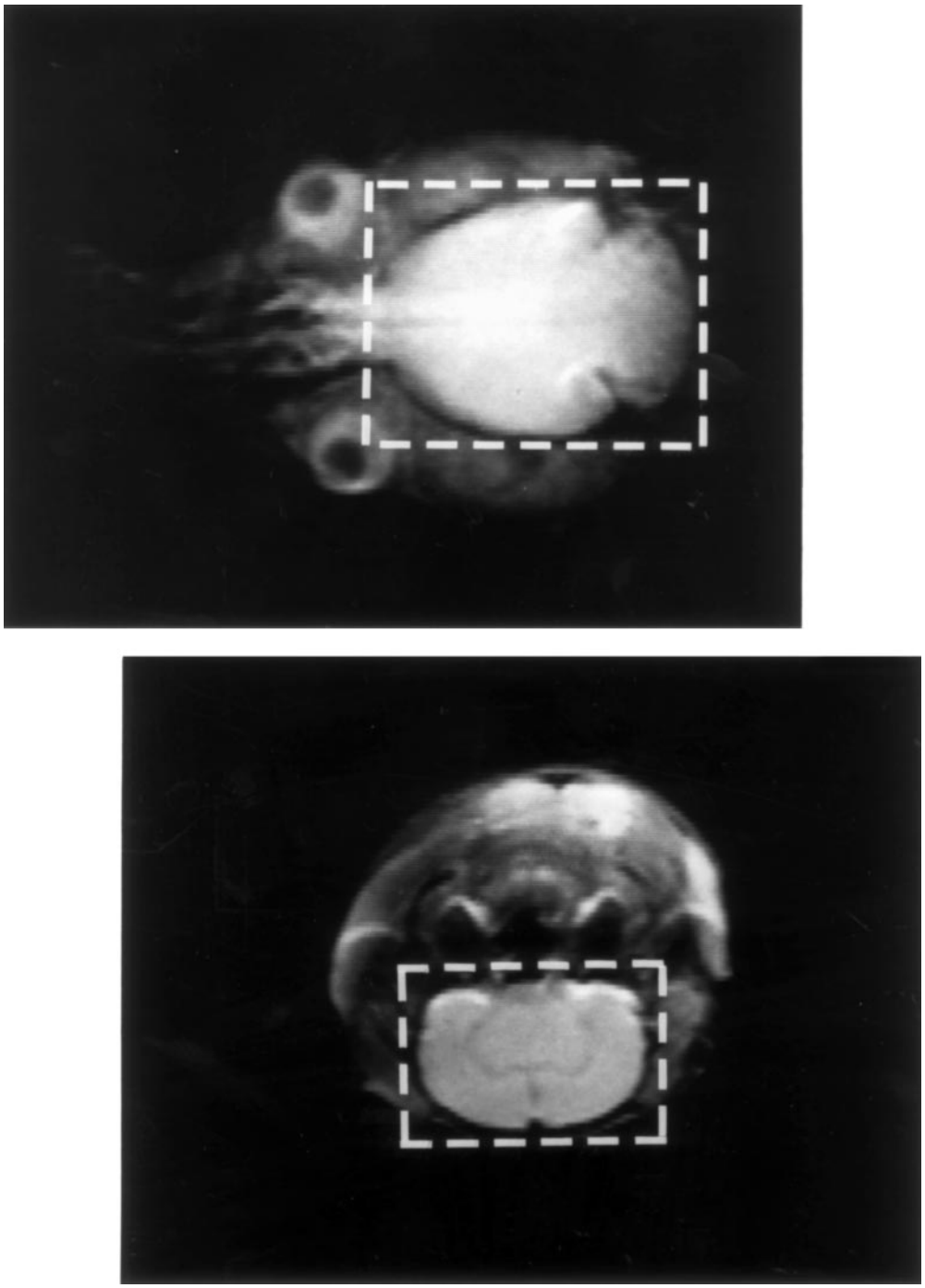

FIG. 5. Proton images of rat brain. *Top:* a transverse image with *x* along the horizontal and *y* along the vertical axis. *Bottom:* a coronal image with *y* along the horizontal and *z* along the vertical axis. The voxel for 3D ISIS, shown by the dotted line, circumscribes the brain and the surrounding skull, which has an average thickness of 1.5 mm.

per unit time of the amide proton H_Z (*9*), to 19 s, which allows complete relaxation of water protons. The signal recovery was 69% for both delays. *In vivo*, the signal recovery was 59 ± 4% (the mean ± sem for three rats) for brain [5-^{15}N]glutamine amide proton H_Z in the 3D-localized spectrum, compared to that in the unlocalized spectrum.

DISCUSSION

Our results show that brain [5-^{15}N]glutamine amide proton H_Z can be selectively observed, with cancellation of all protons not coupled to ^{15}N (except water), in a 3D-localized spectrum from a spontaneously breathing anesthetized rat, using a vol-

TABLE 2
Signal Recovery in Localization for ^{15}N-Coupled Protons in Phantoms and *in Vivo*

VOI (mm)			Signal recovery[a]		
			Phantom		*In vivo*
x	*y*	*z*	ARG proton	GLN amide H_z	Brain [5-^{15}N]GLN amide H_z
26	19	14			59 ± 4 (3)
16	7	7	72		
9	9	9	82 ± 1.6 (2)		
7	7	7	76 ± 2 (3)		
5	5	5	77 ± 0.4 (3)	69 ± 1.5 (3)	

[a] Signal recovery, as defined under Experimental Procedures, is shown as the mean ± sem for the number of determinations (phantoms) or animals (*in vivo*) given in parentheses.

ume probe with homogeneous ^{1}H and ^{15}N fields, and a pulse sequence that combines ISIS with phase-cycled ^{1}H–^{15}N HMQC. The result demonstrates that breathing motion does not interfere with localized selective observation based on a combination of two subtraction methods, ISIS and phase-cycled HMQC. The result is encouraging because susceptibility to motion, resulting in imperfect cancellation of unwanted peaks and coaddition of desired signals, has been considered to be a major drawback of subtraction techniques (*5, 38*). In a normal ^{1}H spectrum of cat brain obtained with a water suppression scheme that optimizes the detection of exchangeable protons, Mori *et al.* (*26*) showed that the largest peaks downfield of water occur at 7.8–8.3 ppm (NAA + nucleosides and proteins). The complete absence of peaks in this region in our 3D-localized *in vivo* spectrum (Fig. 4B) strongly suggests that cancellation of non-^{15}N-coupled protons in the low field region was complete. The signal recovery in the 3D-localized spectra of 72–82% in phantoms and 59 ± 4% *in vivo* (Table 2) shows that ISIS with sinc inversion pulses is an efficient localization technique at ^{1}H frequency. The volume probe used in the present study has the advantages of (a) homogeneous ^{1}H and ^{15}N fields which ensure optimal zero- and double-quantum excitation with conventional (rectangular) ^{15}N pulses and (b) well-defined VOI. Whether better sensitivity can be achieved when a volume probe for transmission is combined with an actively gated surface coil for reception is a question for future investigation.

Water suppression in the *in vivo* spectrum is adequate and shows that the jump–return sequence can be combined with ISIS for water-suppressed observation of exchangeable protons from VOI *in vivo.* However, the following caveat is worth noting. The jump–return sequence is preceded by selective inversion pulses, and the number of inversion pulses in each of the eight ISIS experiments is 0, 1, 2, or 3. Water magnetization in the slices that underwent zero or two inversion pulses is returned to the $+z$ axis by the second ^{1}H pulse (Fig. 1). This magnetization remains unperturbed during the subsequent HMQC sequence. However, water magnetization in the slices that were subjected to one or three inversion pulses, is flipped to the $-z$ axis by the second ^{1}H pulse, and undergoes T_1 relaxation. If TR is short relative to the T_1 of water, partial saturation may occur and be transferred to [5-^{15}N]glutamine amide proton if its exchange rate is fast relative to its T_1. To examine this possibility, signal recovery for [5-^{15}N]glutamine H_z was measured with a TR of 19 s, which allows complete relaxation of water, for comparison with that measured with a TR of 1 s. The signal recovery was virtually the same (69%). The result strongly suggests that attenuation of this amide proton signal does not occur under our experimental condition (pH 7.1, 20°C) because (a) exchange is very slow and/or (b) in our sequence, the water magnetization that does not return to equilibrium with a TR of 1 s represents only one-half of the total water population that supplies exchanging protons. Water suppression by our sequence in rat brain is comparable to that achieved by the OVS–PRESS–WATERGATE sequence for nonselective observation of exchangeable protons in cat brain (*26*). Excellent water suppression has been demonstrated by a gradient-enhanced ^{1}H–^{15}N double-quantum filter *in vitro* (*39*), but this method, with half the intrinsic sensitivity of the phase-cycled method, has not been used for selective observation of ^{15}N-coupled protons *in vivo.*

For selective observation of ^{1}H coupled to ^{13}C, too, ISIS combined with the proton-observed ^{13}C-edited spin-echo method, which is also a combination of two subtraction methods, has been among the most successful in studies of metabolic flux in animal and human brain *in vivo* (*1–3, 10–14*). Taken together, the results strongly suggest that for localized selective observation of protons coupled to ^{15}N or ^{13}C, which are often present at low concentrations *in vivo,* a localization or editing method based on an addition/subtraction scheme is well worth attempting if it predicts the highest sensitivity for the isotopically enriched metabolite of interest. The present study shows that susceptibility to motion, often considered to be a major drawback of ISIS and phase-cycled HMQC, can be overcome even for spontaneously breathing animals.

ACKNOWLEDGMENTS

We are grateful to Dr. James Tropp of GE Medical Systems for expert improvement of the ^{1}H–^{15}N probe which made this work possible, and to Larry Robertson and Rusty Vahle of Bruker Instruments for installation and maintenance of shielded gradients. We thank Robert S. Olsen for taking photographs of the images. K.K. and B.D.R. are Visiting Associates in the Division of Chemistry and Chemical Engineering at California Institute of Technology. This work was supported by Research Grant 2-RO1-NS29048 from the National Institute of Neurological Disorders and Stroke, the U.S. Public Health Service, and an instrumentation grant from the Rudi Schulte Research Institute.

REFERENCES

1. D. L. Rothman, E. J. Novotny, G. I. Shulman, A. M. Howseman, O. A. C. Petroff, G. Mason, T. Nixon, C. C. Hanstock, J. W. Prichard, and R. G. Shulman, ^{1}H–[^{13}C] NMR measurements of [4-^{13}C]glutamate turnover in human brain. *Proc. Natl. Acad. Sci. U.S.A.* **89,** 9603–9606 (1992).
2. F. Hyder, D. L. Rothman, G. F. Mason, A. Rangarajan, K. L. Behar, and R. G. Shulman, Oxidative glucose metabolism in rat brain during single forepaw stimulation: A spatially localized ^{1}H[^{13}C] nuclear magnetic resonance study, *J. Cereb. Blood Flow Metab.* **17,** 1040–1047 (1997).
3. J. W. Pan, G. F. Mason, J. T. Vaughan, W.-J. Chu, Y. Zhang, and H. P. Hetherington, ^{13}C editing of glutamate in human brain using *J*-refocused coherence transfer spectroscopy at 4.1 T, *Magn. Reson. Med.* **37,** 355–358 (1997).
4. M. Terpstra, R. Gruetter, W. B. High, M. Mescher, L. DelaBarre, H. Merkle, and M. Garwood, Lactate turnover in rat glioma measured by in vivo nuclear magnetic resonance spectroscopy, *Cancer Res.* **58,** 5083–5088 (1998).
5. R. E. Hurd and B. K. John, Gradient-enhanced proton-detected heteronuclear multiple-quantum coherence spectroscopy, *J. Magn. Reson.* **91,** 648–653 (1991).
6. P. C. M. van Zijl, A. S. Chesnick, D. DesPres, C. T. W. Moonen, J. Ruiz-Cabello, and P. van Gelderen, In vivo proton spectroscopy and spectroscopic imaging of [1-^{13}C]glucose and its metabolic products, *Magn. Reson. Med.* **30,** 544–551 (1993).
7. R. A. de Graaf, Y. Luo, M. Terpstra, and M. Garwood, Spectral editing with adiabatic pulses, *J. Magn. Reson. B* **109,** 184–193 (1995).
8. A. Bax, R. H. Griffey, and B. L. Hawkins, Correlation of proton and nitrogen-15 chemical shifts by multiple quantum NMR, *J. Magn. Reson.* **55,** 301–315 (1983).
9. K. Kanamori, B. D. Ross, and J. Tropp, Selective *in vivo* observation of [5-^{15}N]glutamine amide protons in rat brain by ^{1}H–^{15}N heteronuclear multiple-quantum-coherence transfer NMR, *J. Magn. Reson B* **107,** 107–115 (1995).
10. S. M. Fitzpatrick, H. P. Hetherington, K. L. Behar, and R. G. Shulman, The flux from glucose to glutamate in the rat brain in vivo as determined by ^{1}H-observed, ^{13}C-edited NMR spectroscopy, *J. Cereb. Blood Flow Metab.* **10,** 170–179 (1990).
11. G. F. Mason, D. L. Rothman, K. L. Behar, and R. G. Shulman, NMR determination of the TCA cycle rate and α-ketoglutarate/glutamate exchange rate in rat brain, *J. Cereb. Blood Flow Metab.* **12,** 434–447 (1992).
12. F. Hyder, J. R. Chase, K. L. Behar, G. F. Mason, M. Siddeek, D. L. Rothman, and R. G. Shulman, Increased tricarboxylic acid cycle flux in rat brain during forepaw stimulation detected by ^{1}H[^{13}C] NMR, *Proc. Natl. Acad. Sci. U.S.A.* **93,** 7612–7617 (1996).
13. D. L. Rothman, K. L. Behar, H. P. Hetherington, J. A. den Hollander, M. R. Bendall, O. A. C. Petroff, and R. G. Shulman, ^{1}H-observe/^{13}C-decouple spectroscopic measurements of lactate and glutamate in the rat brain *in vivo, Proc. Natl. Acad. Sci. U.S.A.* **82,** 1633–1637 (1985).
14. H. P. Hetherington, J. W. Pan, W. J. Chu, G. F. Mason, and B. R. Newcomer, Biological and clinical MRS at ultra-high field, *NMR Biomed.* **10,** 360–371 (1997).
15. K. Kanamori, B. D. Ross, and E. L. Kuo, Dependence of in vivo glutamine synthetase activity on ammonia concentration in rat brain studied by ^{1}H–^{15}N heteronuclear multiple-quantum coherence transfer NMR, *Biochem. J.* **311,** 681–688 (1995).
16. K. Kanamori, B. D. Ross, J. C. Chung, and E. L. Kuo, Severity of hyperammonemic encephalopathy correlates with brain ammonia level and saturation of glutamine synthetase in vivo, *J. Neurochem.* **67,** 1584–1594 (1996).
17. K. Kanamori and B. D. Ross, Glial alkalinization detected in vivo by ^{1}H–^{15}N heteronuclear multiple-quantum coherence-transfer NMR in severely hyperammonemic rat, *J. Neurochem.* **68,** 1209–1220 (1997).
18. K. Kanamori, F. Parivar, and B. D. Ross, A ^{15}N NMR study of in vivo cerebral glutamine synthesis in hyperammonemic rats, *NMR Biomed.* **6,** 21–26 (1993).
19. R. J. Ordidge, A. Connelly, and J. A. B. Lohman, Image-selected *in vivo* spectroscopy (ISIS). A new technique for spatially selective NMR spectroscopy, *J. Magn. Reson.* **66,** 283–294 (1986).
20. R. J. Ordidge, M. R. Bendall, R. E. Gordon, and A. Connelly, Volume selection for *in vivo* biological spectroscopy, *in* "Magnetic Resonance in Biology and Medicine" (G. Govil, C. L. Khetrapal, and A. Saran, Eds.), pp. 387–397, Tata McGraw–Hill, New Delhi (1985).
21. P. A. Bottomley, T. B. Foster, and R. D. Darrow, Depth-resolved surface coil spectroscopy (DRESS) for *in vivo* ^{1}H, ^{31}P and ^{13}C NMR, *J. Magn. Reson.* **59,** 338–342 (1984).
22. J. Granot, Selected volume excitation using stimulated echoes (VEST). Applications to spatially localized spectroscopy and imaging, *J. Magn. Reson.* **70,** 488–492 (1986).
23. J. Frahm, K.-D. Merboldt, and W. Hänicke, Localized proton spectroscopy using stimulated echoes, *J. Magn. Reson.* **72,** 502–508 (1987).
24. R. Kimmich, and D. Hoepfel, Volume-selective multipulse spin-echo spectroscopy, *J. Magn. Reson.* **72,** 379–384 (1987).
25. K. Kanamori, B. D. Ross, and F. Parivar, Selective observation of biologically important ^{15}N-labelled metabolites in isolated rat brain and liver by ^{1}H-detected multiple quantum coherence spectroscopy, *J. Magn. Reson.* **93,** 319–328 (1991).
26. S. Mori, S. M. Eleff, U. Pilatus, N. Mori, and P. C. M. van Zijl, Proton NMR spectroscopy of solvent-saturable resonances: A new approach to study pH effects in situ, *Magn. Reson. Med.* **40,** 36–42 (1998).
27. T. J. Lawry, G. S. Karczmar, M. W. Weiner, and G. B. Matson, Computer simulation of MRS localization techniques: An analysis of ISIS, *Magn. Reson. Med.* **9,** 299–314 (1989).
28. M. Mescher, H. Merkle, J. Kirsch, M. Garwood, and R. Gruetter, Simultaneous *in vivo* spectral editing and water suppression, *NMR Biomed.* **11,** 266–272 (1998).
29. L. Jouvensal, P. G. Carlier, and G. Bloch, Practical implementation of single-voxel double-quantum editing on a whole-body NMR spectrometer: Localized monitoring of lactate in the human leg during and after exercise, *Magn. Reson. Med.* **36,** 487–490 (1996).
30. J. R. Keltner, L. L. Wald, B. B. Frederick, and P. F. Renshaw, In vivo detection of GABA in human brain using a localized double-quantum filter technique, *Magn. Reson. Med.* **37,** 366–371 (1997).
31. J. R. Keltner, L. L. Wald, P. J. Ledden, C. Y. I. Chen, R. T. Matthews, E. H. G. K. Küestermann, J. R. Baker, B. R. Rosen, and B. G. Jenkins, A localized double-quantum filter for the in vivo detection of brain glucose, *Magn. Reson. Med.* **39,** 651–656 (1998).
32. A. Bax, P. G. De Jong, A. F. Mehlkopf, and J. Smidt, Separation of the different orders of NMR multiple-quantum transitions by the use of pulsed field gradients, *Chem. Phys. Lett.* **69,** 567–570 (1980).
33. J. Ruiz-Cabello, G. W. Vuister, C. T. W. Moonen, P. van Gelderen, J. S. Cohen, and P. C. M. van Zijl, Gradient-enhanced hetero-

nuclear correlation spectroscopy. Theory and experimental aspects, *J. Magn. Reson.* **100,** 282–302 (1992).

34. M. Guéron, P. Plateau, and M. Decorps, Solvent signal suppression in NMR, *Prog. NMR Spectrosc.* **23,** 135–210 (1991).

35. H. Bleich, and J. Wilde, Solvent resonance suppression using a sequence of strong pulses, *J. Magn. Reson.* **56,** 154–155 (1984).

36. P. Plateau and M. Guéron, Exchangeable proton NMR without baseline distortion, using new strong-pulse sequences, *J. Am. Chem. Soc.* **104,** 7310–7311 (1982).

37. R. A. De Graaf, Y. Luo, M. Terpstra, H. Merkle, and M. Garwood, A new localization method using an adiabatic pulse, BIR-4, *J. Magn. Reson. B* **106,** 245–252 (1995).

38. J. E. van Dijk, A. F. Mehlkopf, and W. M. M. J. Boveé, Comparison of double and zero quantum NMR editing techniques for in vivo use, *NMR Biomed.* **5,** 75–86 (1992).

39. D. Freeman, N. Sailasuta, S. Sukumar, and R. E. Hurd, Proton-detected ^{15}N NMR spectroscopy and imaging, *J. Magn. Reson.* **102,** 183–192 (1993).

40. F. Blomberg, W. Maurer, and H. Rüterjans, ^{15}N nuclear magnetic resonance investigations on amino acids, *Proc. Natl. Acad. Sci. U.S.A.* **73,** 1409–1413 (1976).

41. N. A. Farrow, K. Kanamori, B. D. Ross, and F. Parivar, An N-15 NMR study of cerebral, hepatic and renal nitrogen metabolism in hyperammonemic rats, *Biochem. J.* **270,** 473–481 (1990).

42. K. Kanamori and B. D. Ross, ^{15}N NMR measurement of the *in vivo* rate of glutamine synthesis and utilization at steady-state in the brain of the hyperammonaemic rat, *Biochem. J.* **293,** 461–468 (1993).

43. G. C. K. Roberts and O. Jardetzky, Nuclear magnetic resonance spectroscopy of amino acids, peptides and proteins, *Adv. Protein Chem.* **24,** 447–545 (1970).

44. R. J. Smith, D. H. Williams, and K. James, Analysis of the rotational motions of the guanidino group in arginine, *J. Chem. Soc. Chem. Commun.,* 682–683 (1989).

45. L. Klevan and D. M. Crothers, High-resolution NMR of exchangeable protons in arginine, oligoarginines and the arginine-rich histone tetramer, *Biopolymers* **18,** 1029–1044 (1979).

46. K. D. Kopple, A. Ahsan, and M. Barfield, Regarding H-C-C(O)–^{15}N coupling as an indicator of peptide torsional angle, *Tetrahedron Lett.* **38,** 3519–3522 (1978).

47. K. Kanamori and B. D. Ross, Localized ^{15}N NMR spectroscopy of rat brain by ISIS, *Magn. Reson. Med.* **41,** 456–463 (1999).

48. N. M. Yongbi, G. S. Payne, D. J. Collins, and M. O. Leach, Quantification of signal selection efficiency, extra volume suppression and contamination for ISIS, STEAM and PRESS localized ^{1}H NMR spectroscopy using an EEC localization test object, *Phys. Med. Biol.* **40,** 1293–1303 (1995).

49. T. Ernst, J. Hennig, D. Ott, and H. Friedburg, The importance of the voxel size in clinical ^{1}H spectroscopy of the human brain, *NMR Biomed* **2,** 216–224 (1989).